Baku State University: Journal of Physics & Space Sciences, **2026**, v3 (1), p. 85-106

journal homepage: http://bsuj.bsu.edu.az/en

The role of L- and D-Histidine in the formation of stable structures of the Cys-His dipeptide

Shahla N. Gadjieva[1], Gultekin Dj. Abbasova[1], Lala I. Veliyeva[2], Irada N. Aliyeva[1*], Lala S. Gadjieva[1]

[1]Department of Optics and Molecular Physics, Baku State University, Baku, Azerbaijan
[2]Department of Chemical Physics of Nanomaterials, Baku State University, Baku, Azerbaijan
R e c e i v e d 10-Feb-2026; A c c e p t e d 19-Mar-2026
DOI: https://doi.org/10.30546/209501.101.2026.3.01.348

Abstract

The work studies the spatial and electronic structure of the Cys-His dipeptide taking into account the isomerization of the histidine residue responsible for the selectivity in binding of the modified Cys-T7 peptide to the transferrin receptor. Interest in this dipeptide stems from its cysteine residue, the thiol group of which is responsible for binding to the drug during its delivery to brain tumor cells. It has also been established that histidine ensures specific receptor recognition and sensitivity to changes in environmental acidity, which is important for drug release. Using semi-empirical methods of molecular mechanics and *ab initio* quantum chemistry method, the effect of L- and D-histidine on the conformational states of the Cys-His dipeptide fragment was studied. A comparative analysis of the obtained results was conducted depending on the methods used, taking into account the parameterization of potential functions. The spatial and electronic structure of the compound under study was defined.

Keywords: Cys-T7 peptide, transferrin receptor, quantum-chemical calculations, electronic structure, molecular dynamics, dipeptide, histidine stereoisomers.
PACS Numbers: 87.15 Aa, 87.15.He, 87.15.By

1. Introduction

It is well known that many cancer cells, such as brain tumors (glioma) affecting the glial cells of the brain or spinal cord, utilize iron–transported by the protein transfer-

[*]*Corresponding author* – Tel.: (+994) 557036545
e-mail address: aliyeva_irada@bsu.edu.az; *ORCID ID*: 0000-0002-5400-6198

rin–to accelerate cell division $[1-3]$. Cancer cells are covered with transferrin receptors, which are actively expressed on the endothelial cells of the blood-brain barrier (BBB). The number of TfR receptors on their surface is 10–100 times higher than on the surface of healthy cells. One of the main challenges in modern neuropharmacology for treating glioma is the blood-brain barrier, which restricts the penetration of more than 98% of potential drug substances into the central nervous system. The transferrin receptor (TfR) is a recognized target for overcoming this barrier $[4-12]$. Numerous studies in recent years $[13-16]$ have established that a peptide molecule consisting of a seven-amino-acid sequence, His-Ala-Ile-Tyr-Pro-Arg-His (or HAIYPRH, with the chemical formula $C_{41}H_{61}ClN_{14}O_9$ and a molecular weight of ~929.46 Da), can act as a ligand capable of binding to transferrin receptors (TfR) while ignoring healthy cells. Studies conducted throughout 2024–2025 have shown that using the T7 peptide modified with cysteine–Cys-His-Ala-Ile-Tyr-Pro-Arg-His (C-HAIYPRH or Cys-T7)-by adding the amino acid cysteine to the N-terminus of the peptide molecule significantly expands its applications in medicine and biotechnology $[17, 18]$. This is because cysteine contains a chemically active sulfhydryl (thiol) group and, through the formation of cysteine bridges, can form strong bonds with high selectivity to maleimide groups on the surface of lipid nanoparticles or polymers, firmly anchoring the peptide to its carrier surface $[18]$.

Experimental studies have established that replacing L-histidine with its mirror isomer, D-histidine, within the Cys-T7 peptide leads to a loss of the molecule's biological activity-specifically, a nearly complete loss of specific binding to the transferrin receptor. Due to this property of amino acid D-stereoisomers, they are frequently used in research laboratories to control the functional activity of drug molecules. If a nanoparticle with the L-peptide penetrates the brain while one with the D-peptide does not, it serves as evidence that transport occurs due to peptide binding and its involvement in receptor activation. Experimental research in this direction has allowed for the determination that the Cys-His fragment at the N-terminus of the Cys-T7 peptide plays a critical role in drug delivery systems and in the processes of binding to the transferrin receptor. In light of the above, the aim of the present study was to investigate the influence of L- and D-histidine on the conformational and electronic characteristics of the Cys-His dipeptide, which is part of the modified octapeptide Cys-T7. Such research is vital for studying the targeted transport of drugs to tissue and organ areas affected by tumors and for understanding the molecular mechanisms of their pharmacological action.

2. Calculation methods

The study of the spatial structure, conformational possibilities, and molecular dynamics of the Cys-His dipeptide–considering both the L- and D-stereoisomers of

histidine–was conducted using molecular mechanics based on the mechanical model of the atom. In molecular mechanics methods, atoms are treated as Newtonian particles within a force field, and the interactions between them are described by semi-empirical potential functions. To describe various types of interactions (non-bonded, electrostatic, torsional, and hydrogen bond formation energy), semi-empirical atom-atom potential functions were utilized, as described in detail in previous work $[24]$. The designations and reference points for rotation angles correspond to the IUPAC-IUB nomenclature [25].

To describe atomic motion and study the conformational and dynamic properties of the investigated compounds in a vacuum and under conditions of explicitly defined water molecules, the molecular dynamics (MD) method was employed. In the MD method, based on the laws of classical mechanics, equations of motion $r = \{r_i(t)\}$ are solved for each atom within the force field of the remaining particles, describing atomic trajectories as a function of time $[26 - 29]$.

Subsequently, potential energy minima corresponding to the metastable configurations of this system in the phase space of particle coordinates are calculated. The result is the construction of a potential energy surface, which includes the statistical equilibrium states of the particle system. The calculation methodology used to search for the global minimum – corresponding to the stable structure of the Cys-His dipeptide with L- and D-stereoisomers of histidine, while maintaining its chemical structure – is described in [27, 28].

To further investigate the effect of isomerization on the electronic characteristics of the dipeptides in more detail, semi-empirical and ab initio quantum chemical methods were utilized [30-34]. These methods allow for the determination of electron density distribution patterns and the occupancy of HOMO (Highest Occupied Molecular Orbital) and LUMO (Lowest Unoccupied Molecular Orbital), as well as the calculation of dipole moments and reactivity descriptors of the dipeptide based on its geometry. Such studies may be useful for study the pathways and mechanisms by which the Cys-T7 peptide binds to the transferrin receptor on the surface of tumor cells.

Quantum-chemical calculations were preceded by determining the coordinates of the equilibrium nuclear configurations in the Cys-His dipeptide. For this purpose, the geometry of the molecule was optimized in the potentials of the PM3 semi-empirical method of molecular mechanics using the Polak-Ribiere algorithm with an accuracy of 0.001 kcal/mol·Å. The resulting data used as the basis for calculating the electronic structure of the dipeptides within the framework of Density Functional Theory (DFT)–an *ab initio* method of quantum chemistry based on fundamental physical constants. According to the Hohenberg-Kohn theorem, all properties of a system in the ground state, including its ground state energy, are determined within this method by its electron density, which depends on only three spatial coordinates, rather than on the $3N$ coordinates of the electrons [30-34].

To describe the exchange-correlation functional, the hybrid three-parameter B3LYP functional (Becke's functional with the Lee-Yang-Parr correlation functional) was used, in which parameters are optimized for the best agreement with experimental atomization or ionization energies. For the calculations, a fairly reliable and time-efficient extended basis set 6-31+G(d,p) was used, taking into account the polarization and diffusion functions. All computations were performed using the Gaussian 09 software package [35]. For the visualization of the results, the GaussView 6.0.16 program was used [36]. The study involved calculating the electronic energy, nuclear repulsion energy, HOMO and LUMO energies, and the energy gap between frontier orbitals. These values allowed for the determination of the ionization potential, electron affinity, and dipole moments, as well as the analysis of the reactivity of the investigated dipeptides.

3. Results and discussion

Spatial structure and conformational states of L-Cys-L-His and L-Cys-D-His dipeptides based on conformational analysis. The specific features of the spatial structure of Cys-His are determined by the chemical structure of the amino acid residues that make up the dipeptide's primary sequence. These include cysteine (α-amino-β-thiopropionic acid) and histidine (L-α-amino- β-imidazolylpropionic acid) with the chemical formula $C_3H_7NO_2S$. Cysteine contains a thiol group, which not only participates in the formation of intramolecular interactions but also acts as an "anchor" for attaching the peptide to nanoparticles or drug. Histidine is a heterocyclic alpha-amino acid containing an imidazole ring, which is capable of changing its charge depending on the pH level. The computational model of the dipeptide, indicating the sequence of amino acid residues and the numbering of atoms in its chemical structure, is shown in Fig. 1.

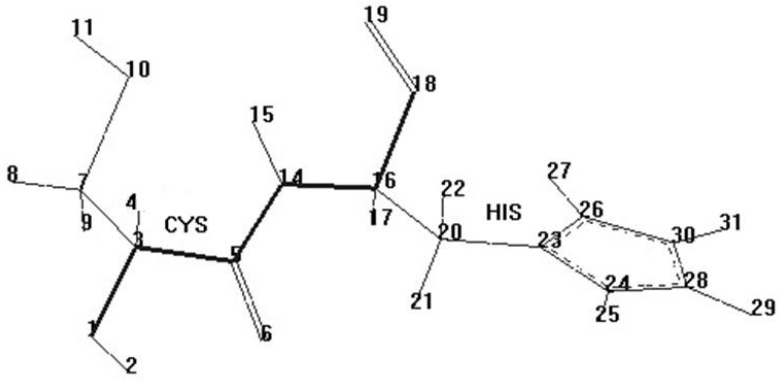

Fig. 1. Calculation model of the Cys-His dipeptide with the sequence of amino acid residues and atom numbering indicated

According to the calculation methodology described in the work [24], the stable structures of L-Cys-L-His and L-Cys-D-His were established based on the low-energy conformations of the cysteine and histidine amino acid residues. The calculations were performed within the framework of a rigid valence scheme for the chemical structure of the dipeptide, specifically taking into account:

(a) the planarity and rigidity of the peptide group;

(b) fixed values for bond angles and bond lengths within the Cys and His amino acid residues.

Tables 1 and 2 present the contributions of various types of interactions, the relative energies, and the dihedral angles of the main chain for the most stable conformational states of the dipeptides containing L- and D-His, corresponding to the folded and extended forms of the peptide chain. As follows from the calculation results, in terms of energy contributions, the most favorable conformations are those with folded structures corresponding to the f −shape of the peptide backbone. However, these structures differ in the forms of the main chain for both cysteine and histidine. As shown in Tables 1 and 2, for L-Cys-L-His, this is the form это RB_3 −, whereas for L-Cys-D-His, the lowest-energy structure corresponds to the BL_2 form of its main chain. Overall, the difference in the total conformational energy between these structures is 1.37 kcal/mol; that is, structures with the L-isomer of histidine are more stable than structures with the D-form of histidine. The contribution from the energy of non-bonded interactions varies within the energy range of $-6.36 \div -6.96\ kcal/mol$ for the L-Cys-L-His dipeptide, and within the range of $-4.44 \div -5.06\ kcal/mol$ for L-Cys-D-His.

The destabilizing contribution from electrostatic interactions is minimal, not exceeding 0.61 kcal/mol for structures with L-His and 0.64 kcal/mol for the dipeptide with D-His. Currently, when describing the conformational possibilities of polypeptide chains, an approach based on Ramachandran plots proves highly effective. According to this method, each amino acid residue is associated with a pair of torsion angles, ϕ (phi) and ψ (psi), at the C^{α} atom. In the structure of polypeptide molecules, including proteins, only the ϕ (phi) and ψ (psi) values that ensure minimum repulsion between the side chains of amino acid residues can be observed. It has been established that for L-amino acids, the energetically favorable zones on the Ramachandran plot are located in the R-region of the conformational space (where negative values for angles ϕ ($N - C^{\alpha}$) and $\psi(C^{\alpha} - C)$ are preferred). For D-His, the preferred areas are the L-regions on the Ramachandran plot (where the ϕ and ψ angles take on positive values). Tables 1 and 2 also show the dihedral angles of the main and side chains for the structures with the minimum total potential energy, including the structure corresponding to the so-called global minimum.

Table 1. Low-energy conformational states of the dipeptide L-Cys-L-His

Form and shape of the main chain*	**Energy components (in kcal/mol)**					**Three-dimensional structure and values of dihedral rotation angles of the main chain**
	E_{nonv}	E_{el}	E_{tors}	E_{total}	E_{rel}	
Folded conformations						
RB_3 f-shape	-6.96	0.49	0.89	-5.57	0.00	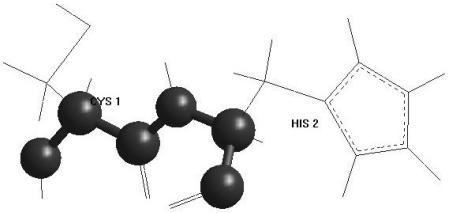 $\varphi_1 = -81.99°, \psi_1 = -176.75°$ $\varphi_2 = -53.78°, \psi_2 = 180.19°$
RR_1 f-shape	-6.45	0.39	1.09	-5.03	0.54	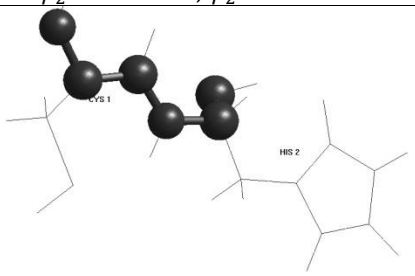 $\varphi_1 = -80.85°, \psi_1 = 177.88°$ $\varphi_2 = -57.35°, \psi_2 = -61.15°$
Extended conformations						
BB_1 e-shape	-6.38	0.61	0.70	-5.07	0.50	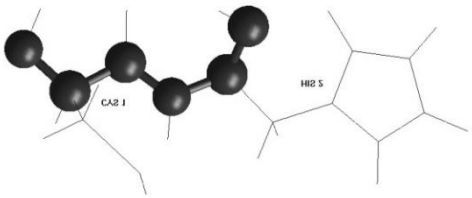 $\varphi_1 = -99.75°, \psi_1 = 181.05°$ $\varphi_2 = -57.78°, \psi_2 = 179.74°$
BB_3 e-shape	-6.36	0.57	0.86	-4.93	0.64	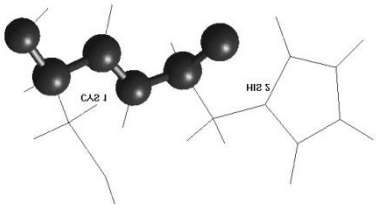 $\varphi_1 = -89.97°, \psi_1 = 182.92°$ $\varphi_2 = -55.51°, \psi_2 = 179.74°$

Table 2. Low-energy conformational states of the dipeptide L-Cys-D-His

Form and shape of the main chain*	**Energy components (in kcal/mol)**					**Three-dimensional structure and values of dihedral rotation angles of the main chain**
	E_{nonv}	E_{el}	E_{tors}	E_{total}	E_{rel}	
Folded conformations						
BL_2 f-shape	-5.06	0.53	0.33	-4.20	0.0	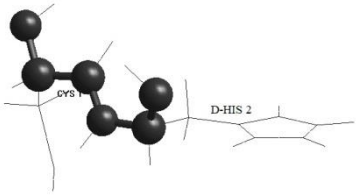 $\varphi_1 = -114.58°, \psi_1 = 175.16°$ $\varphi_2 = 55.93°, \psi_2 = 178.35°$
Extended conformations						
BB_2 e-shape	-4.92	0.58	0.99	-3.35	0.85	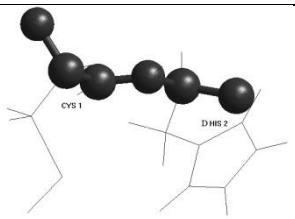 $\varphi_1 = -87.73°, \psi_1 = 110.08°$ $\varphi_2 = -160.47°, \psi_2 = 178.40°$
RL_2 e-shape	-4.44	0.64	0.50	-3.29	0.91	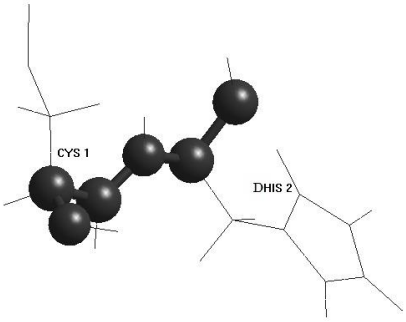 $\varphi_1 = -92.87°, \psi_1 = -98.89°$ $\varphi_2 = 178.46°, \psi_2 = 178.19°$

***In Table 1 and Table 2 subscripts 1,2,3 correspond to the position of the χ angle in the side chain: $\chi_1 = 60°$; : $\chi_2 = 180°$; $\chi_3 = -60°$.

An important role in the formation of stable conformational states belongs to the side chains within the dipeptide structure. It is known that the χ_1 angles determine the positions of the thiol group (-SH) of cysteine and the imidazole ring of

histidine. For cysteine, as with other natural amino acids, particular attention in side-chain conformational analysis is given to the dihedral angle χ_1, which describes rotation around the $C^{\alpha} - C^{\beta}$ bond. The stable states of cysteine are determined by the absence of steric clashes between the sulfhydryl (SH) group in its side chain and the dipeptide backbone. Calculations have shown that in all optimized structures, the cysteine side chain forms weak interactions with the histidine imidazole ring, the energy of which is approximately equal to the energy of dispersion forces ~ -1.55 ккал/моль. In fully extended (unfolded) conformations, the side chains are oriented in opposite directions from the main chain, resulting in minimal interaction between the amino acid radicals. The angle χ_2 in cysteine describes rotation around the $C^{\beta} - C^{\gamma}$ bond. Due to the high polarizability of sulfur, this angle is more labile and can vary over a wider range depending on the presence of hydrogen bonds with the solvent or neighboring residues. It is established that in proteins, cysteine most frequently adopts three stable conformational states–trans and gauche structures with values of 180, +60 and -60^0, respectively–corresponding to local minima on the potential energy surface. The deviations of these angles typically do not exceed $\pm 30°$ from their ideal values.

The conformational mobility of the histidine side chain is determined by two main dihedral angles:

a) rotation around the $C^{\alpha} - C^{\beta}$ bond (angle χ_1),

b) rotation around the $C^{\beta} - C^{\gamma}$ bond (angle χ_2).

The presence of the bulky imidazole ring imposes specific spatial constraints on the structure of the dipeptide. Calculations have shown that while the χ_1 angle in the global conformation of the dipeptide with the L-form of histidine takes on values close to $\pm 60°$, in the low-energy conformation of L-Cys-D-His, the values of this angle vary within the range of $160 \div 180°$, ensuring a trans-configuration of its side-chain atoms. Consequently, this achieves the maximum distance between the imidazole ring and the main chain of the compound, which may have a significant impact on receptor-binding processes.

An important role in conformational calculations belongs to the orientation of the imidazole ring plane relative to the $C^{\beta} - C^{\gamma}$ bond, which is defined by the rotation angleχ_2. As indicated by the results, in the global minimum state, this angle takes a value of $+90.6°$, corresponding to a perpendicular orientation of the imidazole ring. Numerous studies of protein molecular structures indicate that in real proteins, this angle most frequently falls within a wide range of values around $\pm 60 \div \pm 120°$.. This is due to the fact that a parallel orientation of the imidazole ring with respect to neighboring amino acid residues promotes steric clashes and is extremely unfavorable from an energetic standpoint. Studies have shown that replacing L-His with its D-isomer does not have a significant impact on the structure of the main chain; however, it leads to substantial changes in the values of the di-

hedral angles that determine the position of the imidazole ring (Tables 1 and 2). As a result, not only is the position of the ring altered, but its orientation relative to the cysteine residue is also changed. In D-histidine, the side radical (the imidazole ring) is rotated in the opposite direction relative to the dipeptide "backbone" (Fig. 2). Therefore, if the peptide's main chain fits into the receptor pocket correctly, the D-His ring will face "into the wall" or outward, failing to reach the required binding site. Consequently, the peptide will be unable to adopt a conformation complementary to the receptor. These results may explain the essential role of stacking interactions in peptide complexation processes depending on its isomerization.

Figure 2 shows the calculated low-energy conformational states of dipeptides (the numbering corresponds to the conformations shown in Figure 1).

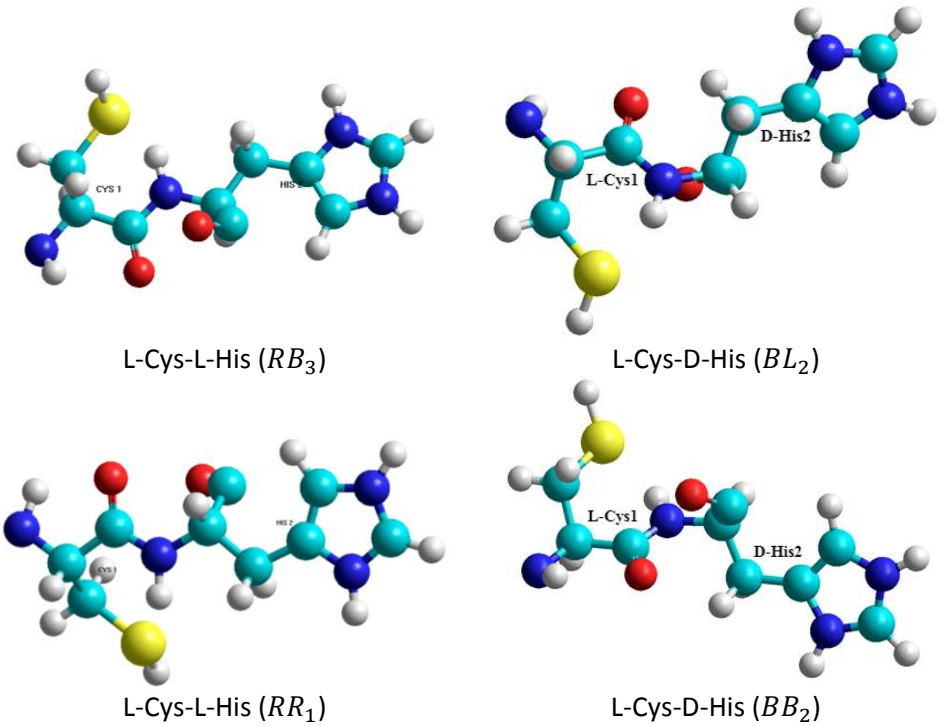

Fig. 2. Stable conformational states of dipeptides according to conformational calculations within the framework of the mechanical model of the atom

Hydrogen bonds play an important role in the functional activity of peptides. It is established that, depending on the pH of the environment, the nitrogen atoms in the histidine ring can act as either donors or acceptors of hydrogen bonds. In an alkaline environment (on the cell surface, where the environment is alkaline with a pH of 7.4), histidine remains neutral. Conversely, inside the cell, where an acidic

environment prevails (pH 5.5), histidine takes up a proton from the medium and becomes positively charged. It is also known that sulfur participates in the formation of weak bonds with the aromatic ring systems of amino acid residues. In such cases, the proton of the cysteine thiol group may be directed toward the center of the aromatic ring. However, the inherent weakness of these bonds often accounts for the flexibility of the polypeptide chains in protein molecules.

Calculation results showed that in L-Cys-L-His, the histidine nitrogen forms a hydrogen bond with the cysteine sulfur $d\ (S-H\ \ldots N_{\delta})$ at a distance of approximately 2.78Å. This bond deviates significantly from linearity, forming an angle of $< N-H\ \ldots S \approx 146{,}6°$. Consequently, the electron cloud of the histidine ring can interact with the lone pairs of electrons on the sulfur atom. The imidazole ring of histidine can also form a hydrogen bond with the NH-group of the peptide bond; however, this bond is very weak and does not contribute significantly to the total energy of the dipeptide. Specifically, the bond length of N-H(His)···O=C(Cys) varies within the range of 2.88–2.98 Å, and its energy does not exceed -0.09 kcal/mol (Table 3). This is primarily due to the electronegativity of the sulfur atom and its relatively large atomic radius. Thus, the system of hydrogen bonds formed, along with their additional contribution to the total conformational energy, further confirms the stability and preference of the folded structures of the dipeptide with L-Histidine compared to L-Cys-D-His.

Table 3. Length (Å) and energy (kcal/mol) of hydrogen bonds in stable conformational states of the dipeptide

Atoms in hydrogen bond	L-Cys-L-His		L-Cys-D-His	
	Bond length	Energy	Bond length	Energy
H-S (Cys)...N-H(His)	2.78	-0.16	-	-
C=O(Cys)...N-H(His)	2.63	-0.24	2.59	-0.27
N-H(His)... C=O(His)	2.71	-0.19	2.59	-0.27
C=O(His)...N-H(NH_2)	2.52	-0.32	2.52	-0.32
N-H (Cys)...O=C(Cys)	2.78	-0.16	2.88	-0.12
C=O(Cys)...H-N(NH_2)	2.07	-1.04	-	-
C=O(C-C=O)...H-N(His)	2.19	-0.78	-	-

Molecular Dynamics of L-Cys-L-His and L-Cys-D-His Dipeptides. One of the most effective approaches used in molecular modeling is the molecular dynamics (MD) method, which is applied to study the properties of systems mimicking biological environments. The MD method offers high spatiotemporal resolution, allowing for the atomic-level study of the structural and physicochemical properties of biological objects and their complexes, as well as the simulation of the complex dynamic

processes occurring within them. Despite significant limitations, this representation can sufficiently describe most events at the molecular level where quantum effects are less significant than electrostatic interactions. Interatomic interaction forces are represented in the form of classical potential forces, defined as the gradient of the system's potential energy.

The objective of this research phase was to study the stability of the resulting dipeptides under conditions simulating the environment with explicitly defined molecules. Since obtaining thermodynamic results and describing the trajectories of system particles does not require long time intervals for such systems, molecular dynamics was conducted over an interval of 0–5 ps. The data obtained from MD served as the basis for describing the conformational dynamics of the dipeptides, the contributions of various energy types, and the equilibrium values of thermodynamic parameters. These results will be used to model the interaction processes of the peptide during the formation of ligand-receptor complexes.

Since the application of classical equations of motion is correct only under conditions where the de Broglie wavelength is much smaller than the size of the atoms and characteristic interatomic distances-a condition met for all atoms in organic substances at room temperature-the calculations were performed at fixed room temperature values. When modeling the aqueous environment, the dimensions of the hypothetical simulation box and the number of water molecules were selected based on the size and compactness of the chosen structures. Table 4 presents the model and dimensions of a hypothetical cube containing 216 water molecules, with a specified minimum distance between the water molecules and the atoms of the dipeptide amino acid residues. Figures 3 and 4 show the structures obtained after the MD simulation.

Table 4. Model of a hypothetical box containing a dipeptide and explicitly defined water molecules in MD simulation

A hypothetical box size	
X	18.70136 Å
y	18.70136 Å
Z	18.70136 Å
Maximum number of water molecules	216
Minimum distance between atoms of a dipeptide and water molecules	2.3Å

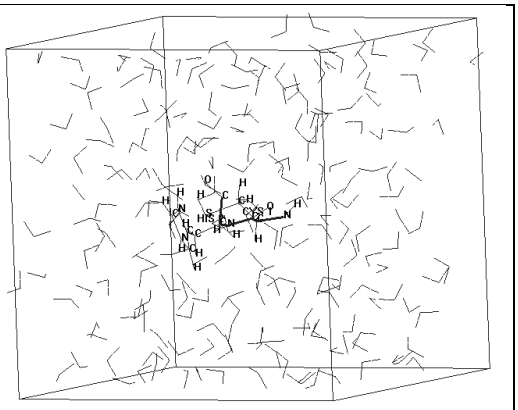

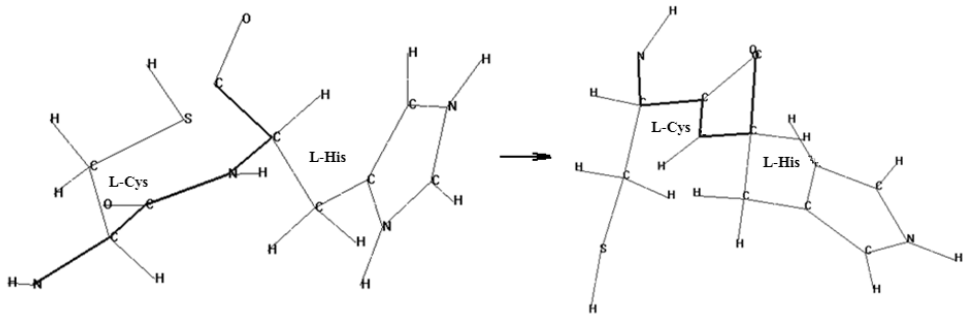

$\Delta E_{kinetic} = 13.11876\, kcal/mol$; $\Delta E_{total} = 4.45822\, kcal/mol$
$\Delta E_{potential} = 15.58076\, kcal/mol$;

Fig. 3. MD simulation of the dipeptide L-Cys-L-His under conditions of explicitly specified water molecules, indicating changes in the values of the energy components (absolute values of decreases are given; relaxation time is 3 ps)

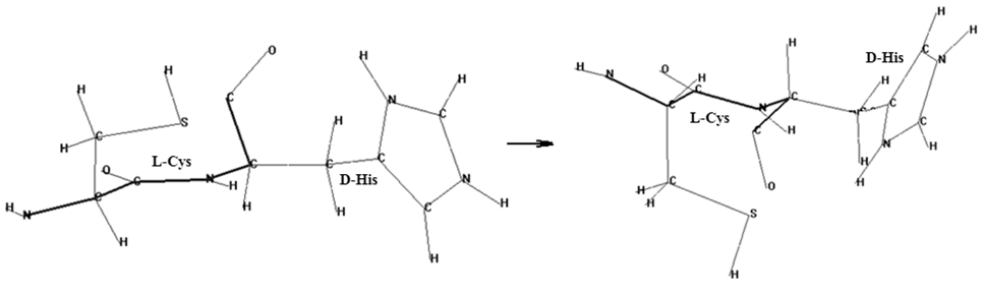

$\Delta E_{kinetic} = 14.0286\, kcal/mol$; $\Delta E_{total} = 3.78077\, kcal/mol$
$\Delta E_{potential} = 15.55803\, kcal/mol$;

Fig. 4. MD simulation of the dipeptide L-Cys-D-His under conditions of explicitly specified water molecules, indicating changes in the values of the energy components (absolute values of decreases are given; relaxation time is 3 ps)

The study results show that despite changes in the energy components indicating relaxation within 3 ps, the folded structures in L-Cys-L-His retained their preference over L-Cys-D-His. These data are consistent with the conformational analysis presented above.

Electronic structure and reactivity parameters of Cys-His with L- and D-Histidine stereoisomers. Further in this work, the electronic structure of the dipeptides was investigated in both the gas phase and aqueous medium using the quantum chemical Density Functional Theory (DFT) method with the hybrid three-parameter B3LYP functional. The DFT/B3LYP method is highly reliable and widely used in the study of biologically active molecules, including peptides. Geometric parameters,

electronic energy values, HOMO and LUMO orbital energies and the resulting energy gap (ΔE), reactivity descriptors, dipole moments, and partial atomic charges were obtained for both environments. The calculations demonstrate that the proposed molecular models form stable structures stabilized by non-covalent interactions. To identify potential binding sites, Molecular Electrostatic Potential (MEP) maps were constructed. Figure 5 illustrates the optimized structures of the Cys-His dipeptide considering the L- and D-isomers of histidine.

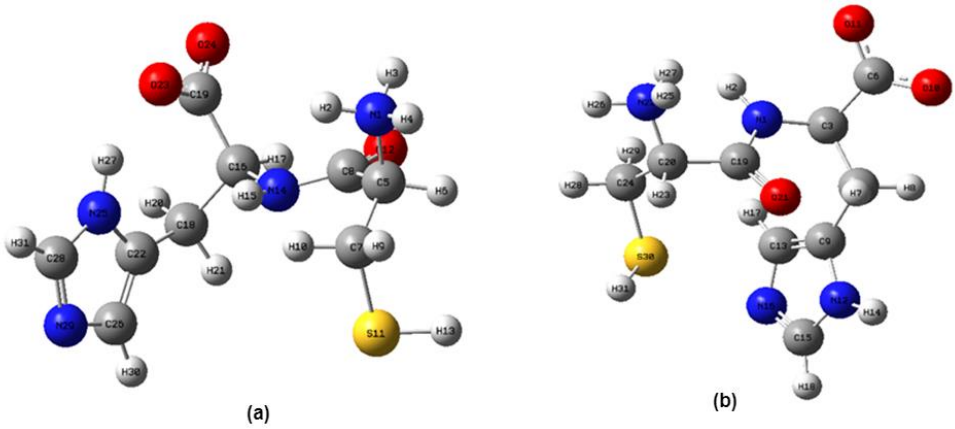

Fig. 5. Optimized structures of dipeptides L-Cys-L-His (a) and L-Cys-D-His (b) at the DFT/B3LYP/6-31+G(d,p) level

Table 5 presents the key energetic and electronic characteristics of the dipeptides obtained from the quantum chemical investigation. These include the total energy, molecular dipole moment, polarizability, and the energies of the frontier molecular orbitals–HOMO (Highest Occupied Molecular Orbital) and LUMO (Lowest Unoccupied Molecular Orbital). Mathematically, the values of the frontier orbital energies can be used to derive global descriptors. These descriptors provide comprehensive chemical information regarding the molecular structure, which correlates with specific molecular properties and proves useful in solving various pharmacological, chemical, and toxicological problems. According to Koopmans' theorem, the first ionization energy is equal to the negative value of the HOMO energy $I = -E_{HOMO}$. Similarly, electron affinity is defined as the negative value of the LUMO energy $A = -E_{LUMO}$. Based on these quantities, several critical indices for predicting molecular activity can be calculated: electronegativity χ=(I+A)/2; chemical potential μ= - (I+A)/2; chemical hardness η=(I-A)/2; hemical softness S=1/2η. Electrophilicity index $\omega=\mu^2/2\eta$ indicates the ability of a molecule to accept electrons from a reagent. Nucleophilicity index $\nu=1/\omega$ is the reciprocal of electrophilicity. Maximum charge transfer $\Delta N=-\mu/\eta$, represents the maximum charge an electrophilic system can accept. The calculation methodology is described in detail in the

following works [37, 38].

Table 5. Energy parameters of dipeptides in the gas phase and aqueous environment

Parameters	L-Cys-L-His		L-Cys-D-His
	Qaz phase	Water solution	Water solution
HOMO (eV)	-6.2826	-6.2292	-6.2889
LUMO (eV)	-0.8237	-0.8405	-0.8577
Energy gap ΔE (eV)	5.4588	5.3887	5.4306
Electron affinity (A)	0.8237	0.8405	0.8577
İonization potential (I)	6.2826	6.2292	6.2889
Electronegativity (χ)	3.5531	3.5348	3.5733
Global hardness (η)	2.7294	2.6943	2.7156
Softness (S)	0.1822	0.1856	0.1844
Chemical potential (μ)	-3.5531	-3.5348	-3.5733
Electrophilicity index (ω)	2.3129	2.3203	2.3509
Nucleophilicity index (υ)	2.83	2.89	2.83
Maksimal elektron transfer (ΔN)	1.300	1.312	1.3158
Dipole moment (Debay)	26.5561	27.1508	14.2664

According to the results of the research (Table 5), in an aqueous environment, the ionization potential of the L-Cys-L-His dipeptide decreases by 0.0534 eV, while the electron affinity increases by 0.0168 eV. The transition from gas phase to water induces several critical changes in the electronic descriptors of the molecule: (a) chemical potential becomes 0.0183 eV less negative; (b) energy gap decreases by 0.0701 eV; (c) chemical hardness decreases by 0.0351 eV; (d) maximum charge transfer increases by 0.012 eV. These fluctuations indicate a slight increase in the molecule's overall chemical reactivity and an enhancement of its electrophilic properties. This is characteristic of a solvent environment where the molecule's capacity to accept electrons is improved. The polarizability which characterizes the deformation of electron density increases significantly in the aqueous phase by 976.31218 eV, further suggesting an increase in chemical activity. The dipole moment is a vital parameter for understanding the electronic behavior and complexation potential of a molecule/ In water, the dipole moment of L-Cys-L-His increases by approximately 0.5947 D, indicating stronger potential for complex formation. A key finding is the comparison between the L- and D-isomers. The dipeptide containing D-His shows a reduction in the dipole moment by 2.8844 D compared to the L-isomer. This substantial decrease provides clear evidence of the diminished reactive capacity of the D-modified peptide.

Table 6 presents the Mulliken atomic charges for the L-Cys-L-His dipeptide in gas and aqueous phases, obtained through optimization at the DFT/B3LYP/6-31+G(d,p) level of theory. It is well-established that Mulliken charges do not represent the

absolute physical distribution of electrical charge between atoms and are notably sensitive to the choice of the basis set. Nevertheless, they serve as a practical tool for the qualitative assessment of charge distribution and for identifying the potential electrophilic and nucleophilic centers susceptible to attack.

Table 6. Partial atomic charges (in units of electron charge) on the atoms of the dipeptide L-Cys-L-His, calculated by the PM3 method and according to the DFT/B3LYP/6-31+G(d,p) calculations

Atom	L-Cys-L-His		
	PM3	DFT (water)	DFT (gas phase)
	Mulliken	Mulliken	Mulliken
N1	0.873593	-0.558183	-0.554630
H2	0.033357	0.413210	0.412908
H3	0.039725	0.414869	0.416912
H4	0.042547	0.414259	0.414073
C5	-0.269250	-0.027009	-0.080531
H6	0.154478	0.242061	0.241008
C7	-0.207920	-0.471931	-0.482559
C8	0.232847	0.183068	0.425757
H9	0.117206	0.232113	0.232239
H10	0.126483	0.229747	0.229956
S11	0.000492	-0.023589	-0.042443
O12	-0.404095	-0.554191	-0.541983
H13	0.036225	0.106985	0.108700
N14	0.042284	-0.109391	-0.140828
H15	0.099256	0.324773	0.303003
C16	-0.128664	-0.428882	-0.436698
H17	0.101815	0.163610	0.164534
C18	-0.002343	-0.439207	-0.669938
C19	0.421663	0.606815	0.516058
H20	0.068640	0.182214	0.183709
H21	0.068324	0.173362	0.174085
C22	-0.309228	0.185460	0.279594
O23	-0.657022	-0.669139	-0.621909
O24	-0.628471	-0.620311	-0.608623
N25	0.305735	-0.282966	-0.298204
C26	-0.160545	-0.154770	-0.073018
H27	0.161446	0.362738	0.369485
C28	-0.245234	0.229003	0.177555
N29	-0.226714	-0.413975	-0.391498
H30	0.142425	0.136278	0.139466
H31	0.170946	0.152979	0.153819

Table 7 presents the optimized values for bond lengths, bond angles, and dihedral angles in L-Cys-L-His. N-H bond lengths vary within the range of 1.02–1.04 Å, C-H bond lengths in the imidazole ring are approximately 1.08 Å, while those in the peptide chain are ~1.08 Å and 1.09 Å. The water environment has virtually no impact on bond lengths; deviations from standard values do not exceed a maximum change of approximately ~0.01 Å.

Table 7. Chemical bond lengths and bond angles in the dipeptide L-Cys-L-His

Chemical bond	**Bond length** (Å)	**Atoms**	**Bond angle (in degree)**
N1-C5	1.51	N1-C5-H4	112.99
N1-H3	1.04	C5-N1-H3	29.61
N1-H2	1.02	C5-N1-H2	26.32
N1-H4	1.02	N1-C5-H5	106.58
C5-H5	1.09	H2-N1-H4	35.96
C5-C8	1.55	C5-C8-O12	117.75
C5-C7	1.54	C5-C7-H6	28.17
C7-H9	1.09	C5-C7-H10	110.74
C7-H10	1.09	C8-O12-N14	124.47
C7-S11	1.83	C8-N14-H15	120.61
C8-O12	1.24	N14-H15-C16	38.34
C8-N14	1.33	N14-C16-H17	108.29
N14-H15	1.01	N14-C16-C19	109.18
N14-C16	1.46	C16-C19-O23	116.38
C16-C19	1.56	C16-C19-O24	116.13
C19-O23	1.27	C16-C18-H20	106.53
C19-O24	1.25	C16-C18-H21	108.75
C16-C18	1.55	H21-C16-C22	106.74
C18-H20	1.09	H20-C16-C22	106.73
C18-H21	1.09	C18-C22-C28	130.99
C18-C22	1.50	C18-C22-N25	124.27
C22-C26	1.38	C22-N25-H27	121.69
C26-H30	1.08	C22-N25C28	107.81
C26-N29	1.38	H27-N25-C28	128.04
N29-C28	1.32	N25-C28-H31	122.43
C28-H31	1.08	N25-C28-N29	111.66
C28-N25	1.38	H31-C28-N29	125.99
N25-H27	1.02	C28-N29-C26	105.00
N25-C22	1.38	N29-C26-H30	121.69
		H30-C26-C22	127.55

Interactions between hydrogen atoms and oxygen or nitrogen atoms lead to the formation of non-covalent intramolecular interactions between non-bonded atoms. Table 8 presents several interactions that can be classified as weak hydrogen bonds for the dipeptide under study.

Table 8. Hydrogen bond parameters in L-Cys-L-His. Bond lengths between donor (D), acceptor (A), and hydrogen (H) are given in Å.

Atoms	H…A	D…A	∠DHA (degree)
N14-H15…O12	2.27	3.18	147.36
N1-H4…O12	2.53	3.31	132.76
N14-H17…O23	2.70	3.23	56.20
N14-H17…O24	3.55	2.53	100.33
N25-H27…O23	2.84	1.91	148.52

Using molecular modeling software, it is possible to obtain a visual three-dimensional representation of the electronic properties of the compounds under study, which is highly effective for analysis. Figure 6 illustrates the HOMO and LUMO orbitals, along with their energy difference, for the dipeptide molecules in both the gas phase and aqueous medium, calculated at the same level of theory. These visualizations allow for the identification of specific regions within the molecular orbitals where electronic transitions occur. The red color in the figure indicates regions of electron density (negative charge), while the green color indicates regions of electron deficiency (positive charge). As seen in Figure 6, the HOMO of the dipeptide in the gas phase is primarily localized on the bonds of the imidazole ring within the histidine fragment of the molecule. Upon transitioning to the LUMO orbital, the amine group becomes completely vacant, and the electron density becomes concentrated over the hydrogen atoms of the imidazole ring and the hydrogen atom of the peptide bond.

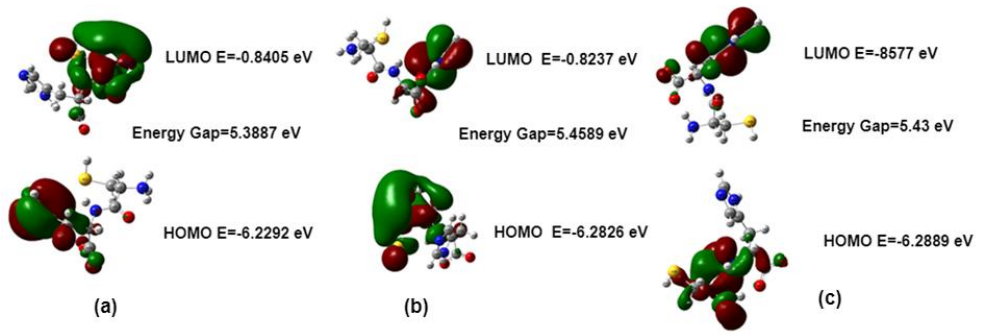

Fig. 6. HOMO and LUMO of the dipeptide L-Cys-L-His in (a) the gas phase and (b) an aqueous medium and (c) L-Cys-D-His in an aqueous medium

The analysis of frontier molecular orbitals, due to their accessibility to electrophiles and nucleophiles, respectively, provides a clear insight into the chemical properties of molecules. The sign of the Lowest Unoccupied Molecular Orbital (LUMO) energy determines whether a molecule behaves as an electrophilic or nucleophilic reagent. It is nucleophiles if the LUMO energy is positive and electrophiles if the LUMO energy is negative. According to our calculations, the dipeptide is conventionally classified as an electrophile. The energy gap between the ground state (HOMO) and the excited state (LUMO) provides critical information regarding structural stability. Generally, a smaller energy gap indicates higher chemical and biological activity of the investigated compound. Calculations show that in an aqueous medium, the HOMO-LUMO energy gap decreases by 0.0701 eV. Comparing this value with the L-Cys-D-His dipeptide revealed an increase in the gap ΔE size, confirming that this isomer is less reactive than L-Cys-L-His.

Molecular Electrostatic Potential (MEP) is considered the most informative descriptor for analyzing molecular interactions. MEP surfaces visualize the three-dimensional distribution of charge within a molecule, allowing researchers to predict chemical reactivity and identify specific docking sites during complexation. The MEP is typically mapped onto a surface of constant electron density (an isodensity surface). This mapping uses a color-coded gradient to represent the electrostatic potential as follows:

(a) red and yellow regions indicate low potential (negative charge) areas; they are characterized by an abundance of electrons, making them the primary targets for electrophilic attack;

(b) blue regions indicate high potential (positive charge) areas; they represent a relative deficiency of electrons, marking them as favorable sites for nucleophilic attack;

(c) green regions represent neutral or zero potential areas.

By analyzing these maps, one can visually determine how the dipeptide will orient itself when approaching a receptor, as well as which specific atoms (such as the nitrogen in the imidazole ring or the sulfur in the cysteine side chain) will act as the primary points of interaction.

Figure 7 displays the MEP maps for the L-Cys-L-His dipeptide molecule, calculated using the DFT/B3LYP/6-31+G(d,p) method in both gas and aqueous environments. As observed, the most active reactive centers of the dipeptide are the oxygen atoms of the carboxyl and peptide groups. Additionally, the nitrogen atoms (N) of the imidazole ring and the amine group are susceptible to electrophilic attack (indicated in yellow). A pronounced blue color is localized over the cysteine atoms, including its thiol group (S-H). This serves as a visual confirmation of the high reactivity of this group during complexation processes.

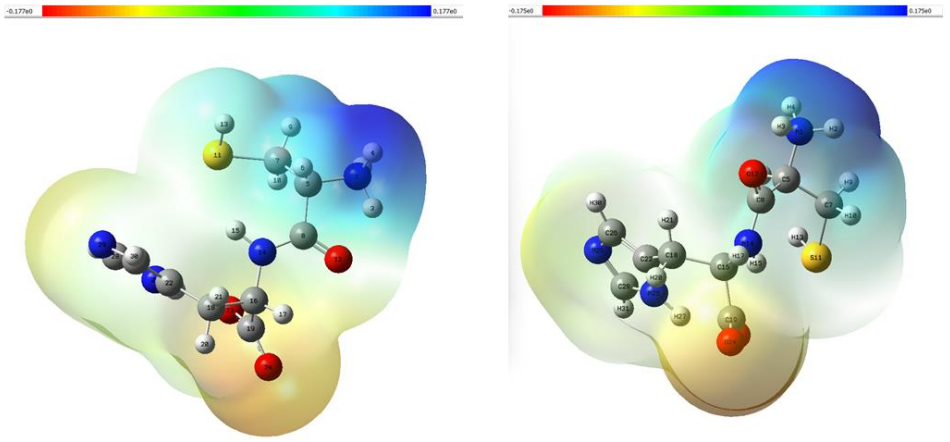

Fig. 7. MEP of the dipeptide L-Cys-L-His for the gas phase (left) and water (right) environment

4. Conclusion

In summary, based on the results of this study, it can be concluded that the replacement of L-histidine with its D-isomer in the Cys-His dipeptide destabilizes the structure in terms of both energetic and electronic characteristics. This is primarily reflected in the reactivity descriptors of the dipeptide. The dipeptide possesses three main regions involved in the formation of stable ligand-receptor complexes: (a) dispersion interactions of the histidine imidazole ring; (b) electrostatic interactions of charged atomic groups in both the peptide backbone and the side chains; (c) the hydrogen bonding system. The study demonstrates that the formation of extended (unfolded) conformational states for L-Cys-D-His is accompanied by a loss of hydrogen bonding contributions (~1.5 kcal/mol) and π –stacking interactions (~1.5 kcal/mol). It is well-established that sulfur within the thioether group plays a vital role in ligand-receptor interactions. Its high polarizability allows it to stabilize histidine conformations, which is critical for effective binding. The substitution of L-His with D-His can lead to a weakening of its participation in intermolecular contacts. These results align with experimental data indicating that proteolytic enzymes in the blood are specifically "tuned" to L-isomers. Consequently, peptides containing D-His may exhibit high metastability and remain in the bloodstream longer without binding to the transferrin target. Due to their conformational mobility, spatial features, and unique electronic structure, D-modified peptide carriers–including the Cys-T7 peptide–are frequently used in laboratory settings as negative controls. If a nanoparticle conjugated with an L-peptide penetrates the brain while the D-peptide variant does not, it provides definitive proof that delivery oc-

curs specifically via receptor-mediated transport rather than simple physicochemical adhesion to membranes. The results of this study will be instrumental in further investigating the spatial structure and electronic characteristics of the T7 peptide and its cysteine-modified variant, Cys-T7, which exhibits a higher affinity for transferrin targets.

References

[1] Koneru, T.; McCord, E.; Pawar, S.; Tatiparti, K.; Sau, S.; Iyer, A.K. Transferrin: Biology and use in receptor-targeted nanotherapy of gliomas. Review. *ACS Omega* **2021**, *6 (13)*, pp. 8727–8733, DOI: 10.1021/acsomega.0c05848.

[2] Davis, M.E. Glioblastoma: Overview of disease and treatment. Review. *Clin. J. Oncol. Nurs.* **2016**, *20 (5 Suppl)*, pp. S2-8, DOI: 10.1188/16.CJON.S1.2-8.

[3] Zhao, M.; van Straten, D.; Broekman, M.L.D.; Préat, V.; Schiffelers, R.M. Nanocarrier-based drug combination therapy for glioblastoma. *Theranostics* **2020**, *10 (3)*, pp. 1355–1372, DOI: 10.7150/thno.38147.

[4] Ghosh, D.; Peng, X.; Leal, J.; Mohanty, R.P. Peptides as drug delivery vehicles across biological barriers. *J. Pharm. Investig.* **2017**, *48 (1)*, pp. 89-111, DOI: 10.1007/s40005-017-0374-0.

[5] Lee, J.H.; Engler, J.A. et al. Receptor mediated uptake of peptides that bind the human transferrin Receptor. *Eur. J. Biochem.* **2001**, *268*, pp. 2004-2012, DOI: 10.1046/j.1432-1327.2001.02073.x.

[6] Guan, Z.H.; Wen, J.L. Peptide-Functionalized Nanoparticles-Encapsulated Cyclin-Dependent Kinases Inhibitor Seliciclib in Transferrin Receptor Overexpressed Cancer Cells. *Nanomaterials (Basel)* **2021**, *11(3)*, p. 772, DOI: 10.3390/nano11030772.

[7] McQuaid, C.; Halsey, A.; Dubois, M.; Romero, I.; Male, D. Comparison of poly-peptides that bind the transferrin receptor for targeting gold nanocarriers. *PLoS One* **2021**, *16(6)*, e0252341, DOI: 10.1371/journal.pone.0252341.

[8] Backer, P.B.; Adesina, S.K. Synthesis and Characterization of Transferrin Receptor-Targeted Peptide Combination SN-38 and Rucaparib Conjugate for the Treatment of Glioblastoma. *Pharmaceutics* **2025**, *17(6)*, p. 732, DOI: 10.3390/pharmaceutics17060732.

[9] Tang, J.; Wang, Q. et al. Stabilized Retro-Inverso Peptide Ligand of Transferrin Receptor for Enhanced Liposome-Based Hepatocellular Carcinoma-Targeted Drug Delivery. *Acta Biomaterialia* **2019**, *83*, pp. 379-389, DOI: 10.1016/j.actbio.2018.11.002.

[10] Yu, J.; Mao, X.; Yang, X.; Zhao, G.; Li, S. New Transferrin Receptor-Targeted Peptide–Doxorubicin Conjugates: Synthesis and In Vitro Antitumor Activity. *Molecules* **2024**, *29(8)*, p. 1758, DOI: 10.3390/molecules29081758.

[11] Hoppenz, P.; Els-Heindl, S.; Beck-Sickinger, A.G. Peptide-drug conjugates and their targets in advanced cancer therapies. *Front. Chem.* **2020**, *8*, p. 571, DOI: 10.3389/fchem.2020.00571.

[12] Chavda, V.P.; Solanki, H.K.; Davidson, M.; Apostolopoulos, V.; Bojarska, J. Peptide-drug

conjugates: A new hope for cancer management. Review. *Molecules* **2022**, *27 (21)*, p. 7232, DOI: 10.3390/molecules27217232.

[13] Cheng, X.; Yu, D.; Cheng, G.; Yung, B.C.; Liu, Y.; Li, H.; Kang, C.; Fang, X.; Tian, S.; Zhou, X. et al. T7 peptide-conjugated lipid nanoparticles for dual modulation of Bcl-2 and Akt-1 in lung and cervical carcinomas. *Mol. Pharm.* **2018**, *15(10)*, pp. 4722-4732, DOI: 10.1021/acs.molpharmaceut.8b00696.

[14] Liu, F.; Wang, F.; Dong, X.; Xiu, P.; Sun, P.; Li, Z.; Shi, X.; Zhong, J. T7 peptide cytotoxicity in human hepatocellular carcinoma cells is mediated by suppression of autophagy. *Int. J. Mol. Med.* **2019**, *44(2)*, pp. 523-534, DOI: 10.3892/ijmm.2019.4231.

[15] Kuang, Y.; An, S.; Guo, Y.; Huang, S.; Shao, K.; Liu, Y.; Li, J.; Ma, H.; Jiang, C. T7 peptide-functionalized nanoparticles utilizing RNA interference for glioma dual targeting. *Int. J. Pharm.* **2013**, *454(1)*, pp. 11-20, DOI: 10.1016/j.ijpharm.2013.07.019.

[16] Kang, Z.; Zeng, C.; Tian, L.; Wang, T.; Yang, S.; Cheng, Q.; Zhang, J.; Meng, Q.; Zhang, C.; Meng, Z. Transferrin receptor targeting segment T7 containing peptide gene delivery vectors for efficient transfection of brain tumor cells. *Drug Deliv.* **2022**, *29(1)*, pp. 2375-2385, DOI: 10.1080/10717544.2022.2102696.

[17] Zong, T.; Mei, L.; Gao, H.; Shi, K.; Chen, J.; Wang, Y.; Zhang, Q.; Yang, Y.; He, Q. Enhanced glioma targeting and penetration by dual-targeting liposome co-modified with T7 and TAT. *J. Pharm. Sci.* **2014**, *103 (12)*, pp. 3891–3901, DOI: 10.1002/jps.24186.

[18] Kuang, Y.; An, S.; Guo, Y.; Huang, S.; Shao, K.; Liu, Y.; Li, J.; Ma, H.; Jiang, C. T7 peptide-functionalized nanoparticles utilizing RNA interference for glioma dual targeting. *Int. J. Pharm.* **2013**, *454 (1)*, pp. 11-20, DOI: 10.1016/j.ijpharm.2013.07.019.

[19] Zhang, S.S.; Yu, J.H. et al. T7 peptide-mediated co-delivery platform overcoming multi-drug-resistant breast cancer: In vitro and in vivo evaluation. *Eur. J. Pharm. Biopharm.* **2024**, *200*, 114327, DOI: 10.1016/j.ejpb.2024.114327.

[20] Li, S.; Wang, R.; Li, J.; Liu, Y.; Fu, Y.; Zhou, J.; Yang, G.; Shan, Y. Revealing the Dynamic Mechanism by Which Transferrin Promotes the Cellular Uptake of HAIYPRH Peptide-Conjugated Nanostructures by Force Tracing. *Mol. Pharm.* **2021**, *18 (3)*, pp. 1480−1485, DOI: 10.1021/acs.molpharmaceut.0c01119.

[21] Wang, M.; Liu, J.; Xia, M.; Yin, L.; Zhang, L.; Liu, X.; Cheng, Y. Peptide-drug conjugates: A new paradigm for targeted cancer therapy. *Eur. J. Med. Chem.* **2024**, *265*, 116119, DOI: 10.1016/j.ejmech.2023.116119.

[22] Wei, G.; Wang, Y.; Yang, G.; Wang, Y.; Ju, R. Recent progress in nanomedicine for enhanced cancer chemotherapy. *Theranostics* **2021**, *11(13)*, pp. 6370–6392, DOI: 10.7150/thno.57828.

[23] Sun, X.; Xie, D.; Lou, Z.; Zhou, Y.; Li, M.; Cai, Y. T7 Peptide-modified macrophage membrane-coated nanoplatform for enhanced glioma treatment. *Eur. J. Pharm. Biopharm.* **2024**, *204*, 114527, DOI: 10.1016/j.ejpb.2024.114527.

[24] Popov, E.M. *Structural Organization of Proteins*; Nauka: Moscow, **1989**; 352 p. (in Russian).

[25] IUPAC-IUB. *Quantities, Units and Symbols in Physical Chemistry*; Blackwell Scientific:

Oxford, **1993**; 166 p.

[26] Karplus, M.; McCammon, J.A. Molecular dynamics simulations of biomolecules. *Nat. Struct. Biol.* **2002**, *9 (9)*, pp. 646-652, DOI: 10.1038/nsb0902-646

[27] Agafonov, A.N.; Eremin, A.V. *Method of Classical Molecular Dynamics in Modeling of Physical and Chemical Processes*; Samara University Publishing House: Samara, **2017**; 68 p. (in Russian).

[28] Aksenova, E.V.; Kshevetsky, M.S. *Computational Methods for the Study of Molecular Dynamics*; SPbSU: St. Petersburg, **2009**; 50 p. (in Russian).

[29] Hernández-Rodríguez, M.; Rosales-Hernández, M.C.; Mendieta-Wejebe, J.E.; Martínez-Archundia, M.; Basurto, J.C. Current Tools and Methods in Molecular Dynamics (MD) Simulations for Drug Design. *Curr. Med. Chem.* **2016**, *23(34)*, pp. 3909-3924, DOI: 10.2174/0929867323666160530144742.

[30] Harrison, N.M. *An Introduction to Density Functional Theory*; Imperial College of Science Technology and Medicine: London, **2001**; 26 p.

[31] Koch, W.A.; Holthausen, M.C. *A Chemist's Guide to Density Functional Theory*; Wiley-VCH Verlag GmbH: Weinheim, **2001**; 306 p. DOI: 10.1002/3527600043.

[32] Kohn, W.A.; Becke, A.D.; Parr, R.G. Density Functional Theory of Electronic Structure. *J. Phys. Chem.* **1996**, *100*, pp. 12974-12980, DOI: 10.1021/jp960669l.

[33] von Barth, U. Basic Density-Functional Theory-an Overview. *Physica Scripta* **2004**, *T109*, pp. 9-39.

[34] Shklovsky, A.G.; Beregovoy, A.V. *Density Functional Theory for Atoms and Simple Molecules*; NRU BelSU: Belgorod, **2014**; 189 p. (in Russian).

[35] Frisch, M.J. et al. *Gaussian 09, Revision D.01*; Gaussian, Inc.: Wallingford, CT, **2013**.

[36] Dennington, R.; Todd, A.K.; Millam, J.M. *GaussView, Version 6.0*; Semichem Inc.: Shawnee Mission, KS, **2016**.

[37] Demukhamedova, S.D.; Aliyeva, I.N. Computer simulation of the structure of some azo-derivatives of β diketones by the methods of quantum chemistry. *New Materials, Compounds and Applications* **2024**, *8(1)*, pp. 24-42, DOI: 10.62476/nmca8124.

[38] Gurbanov, A.V.; Kuznetsov, M.L.; Demukhamedova, S.D.; Alieva, I.N.; Godjaev, N.M.; Zubkov, F.I.; Mahmudov, K.T.; Pombeiro, A.J.L. Role of substituents on resonance assisted hydrogen bonding vs. intermolecular hydrogen bonding. *CrystEngComm* **2020**, *22*, pp. 628-633, DOI: 10.1039/C9CE01744E.